Supplementary Information: Optical reconfiguration and polarization control in semi-continuous gold films close to the percolation threshold

Christian Frydendahl[1,2], Taavi Repän[1], Mathias Geisler[1,2], Sergey M. Novikov[3], Jonas Beermann[3], Andrei Lavrinenko[1], Sanshui Xiao[1,2], Sergey I. Bozhevolnyi[3], N. Asger Mortensen[1,2,3] & Nicolas Stenger[1,2]

[1]*Department of Photonics Engineering, Technical University of Denmark, Ørsteds Plads 343, DK-2800 Kongens Lyngby, Denmark*

[2]*Center for Nanostructured Graphene, Technical University of Denmark, Ørsteds Plads 343, DK-2800 Kongens Lyngby, Denmark*

[3]*Centre for Nano Optics, University of Southern Denmark, Campusvej 55, DK-5230 Odense M, Denmark*

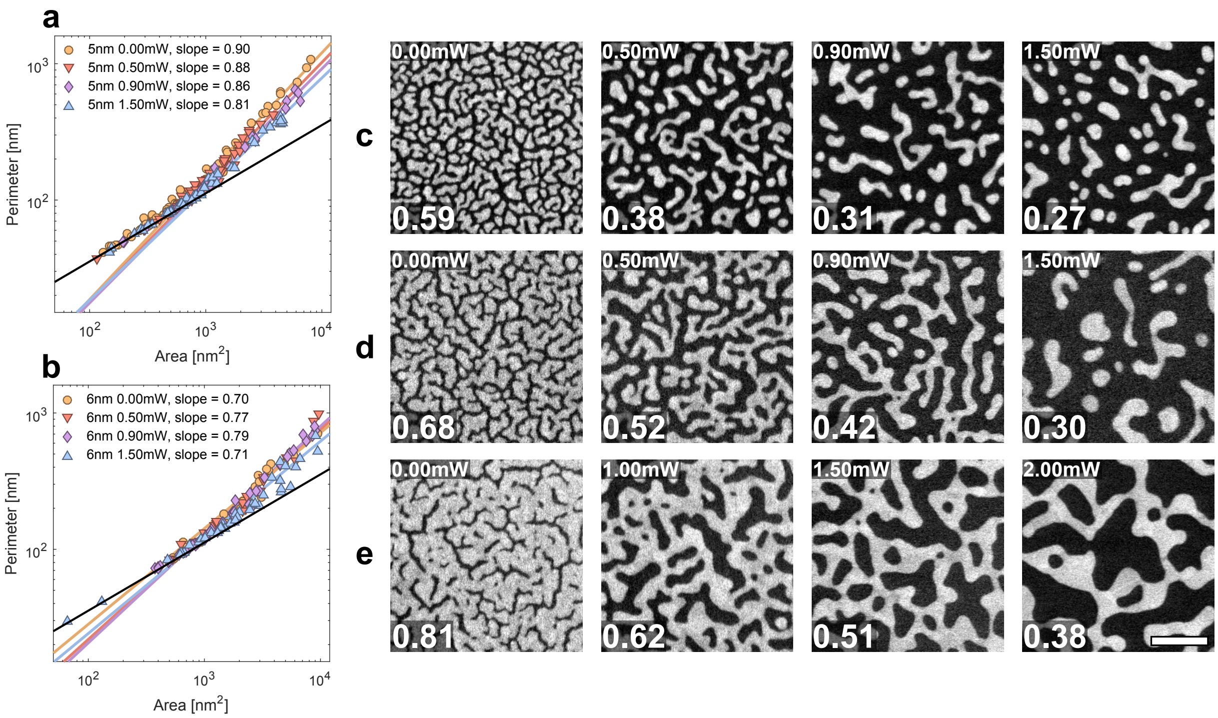

Supplementary Figure 1: Sample morphologies. Area vs. perimeter plots of particles in HAADF images of the **(a)** 5 nm, and **(b)** 6 nm films before and after optical illumination. Slopes of linear fits are indicated and the full black lines are for perfectly separated circular particles. Because the 7 nm film consists of a fully interconnected film with only gaps, a similar plot cannot be produced for it. HAADF images of gold films, **(c)** 5 nm, **(d)** 6 nm, **(e)** 7 nm. The numbers in the lower left corners of the images indicate found filling fractions of gold, numbers in the upper left corners are the laser power used for illumination, and for all samples a wavelength of 740 nm was used. All images at same scale, the scale bar is 150 nm.

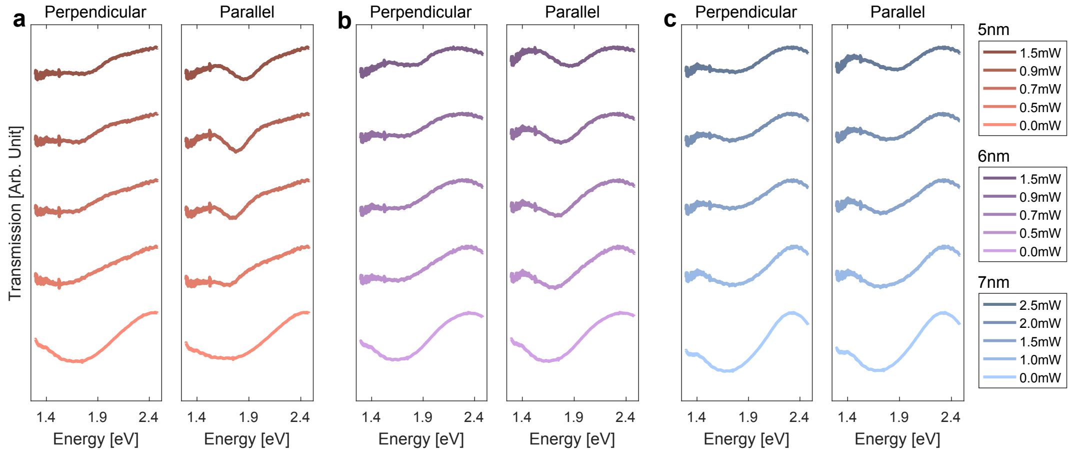

Supplementary Figure 2: Transmission spectra. Full transmission data from the **(a)** 5 nm, **(b)** 6 nm, and **(c)** 7 nm samples. The light source was either polarized parallel or perpendicular to the polarization of the laser used for the reconfiguration.

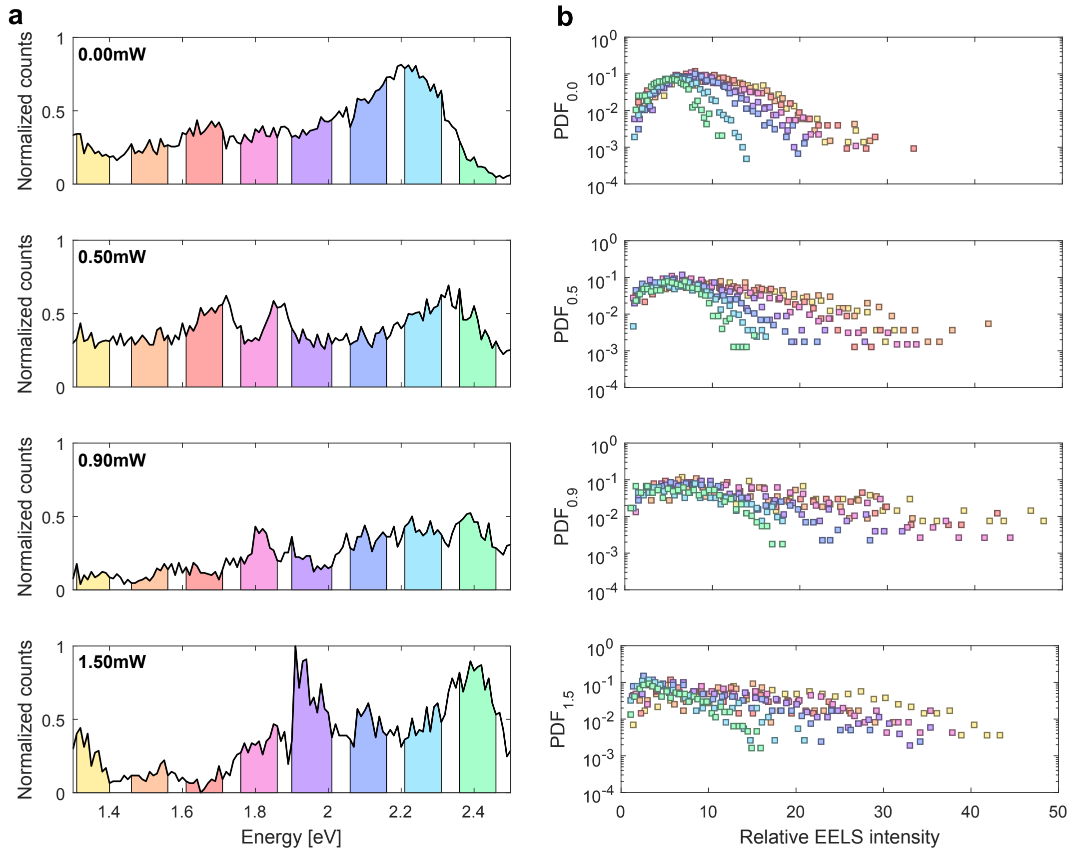

Supplementary Figure 3: Mode distribution 5 nm. **(a)** Normalized histograms of identified central energies of plasmonic peaks from the full spectral image of the 5 nm film with different powers of optical illumination. **(b)** PDFs of relative EELS intensities. The dataset of **(a)** has been discretized into several 0.1 eV windows, and PDFs have been constructed from the intensities of peaks in these ranges.

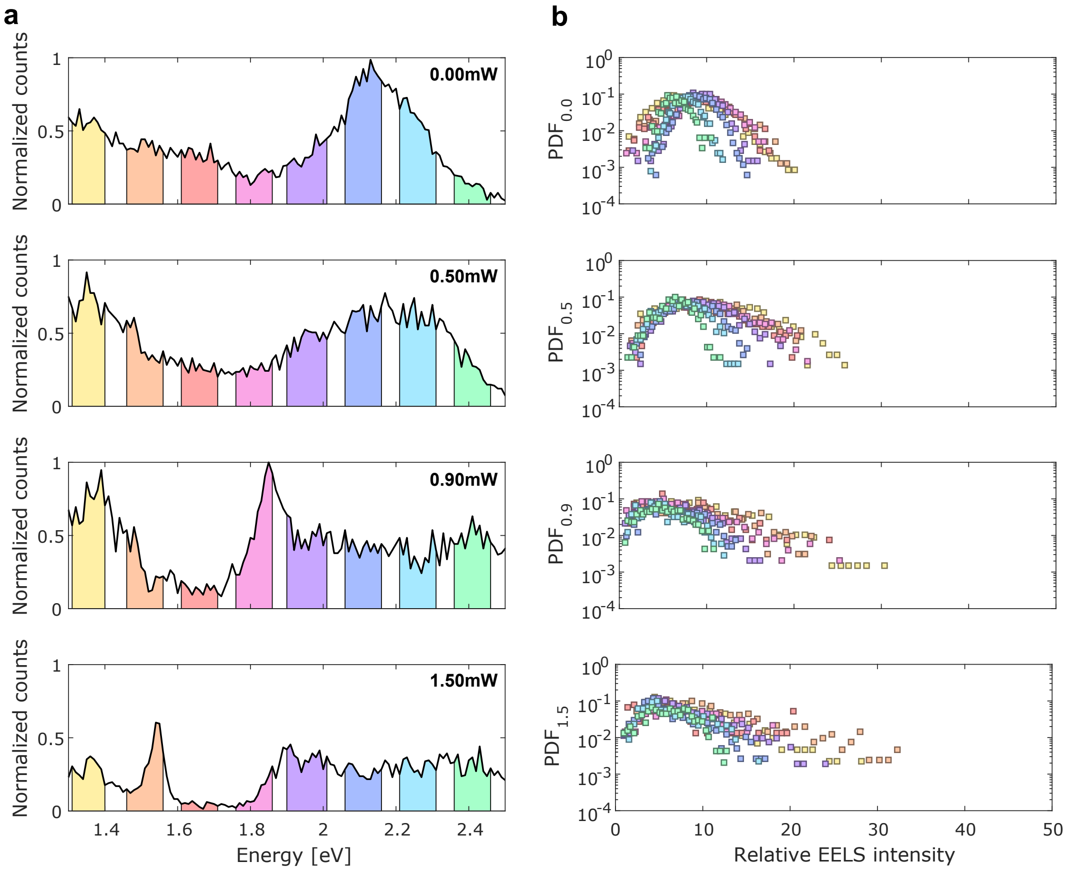

Supplementary Figure 4: Mode distribution 6 nm. **(a)** Normalized histograms of identified central energies of plasmonic peaks from the full spectral image of the 6 nm film with different powers of optical illumination. **(b)** PDFs of relative EELS intensities. The dataset of **(a)** has been discretized into several 0.1 eV windows, and PDFs have been constructed from the intensities of peaks in these ranges.

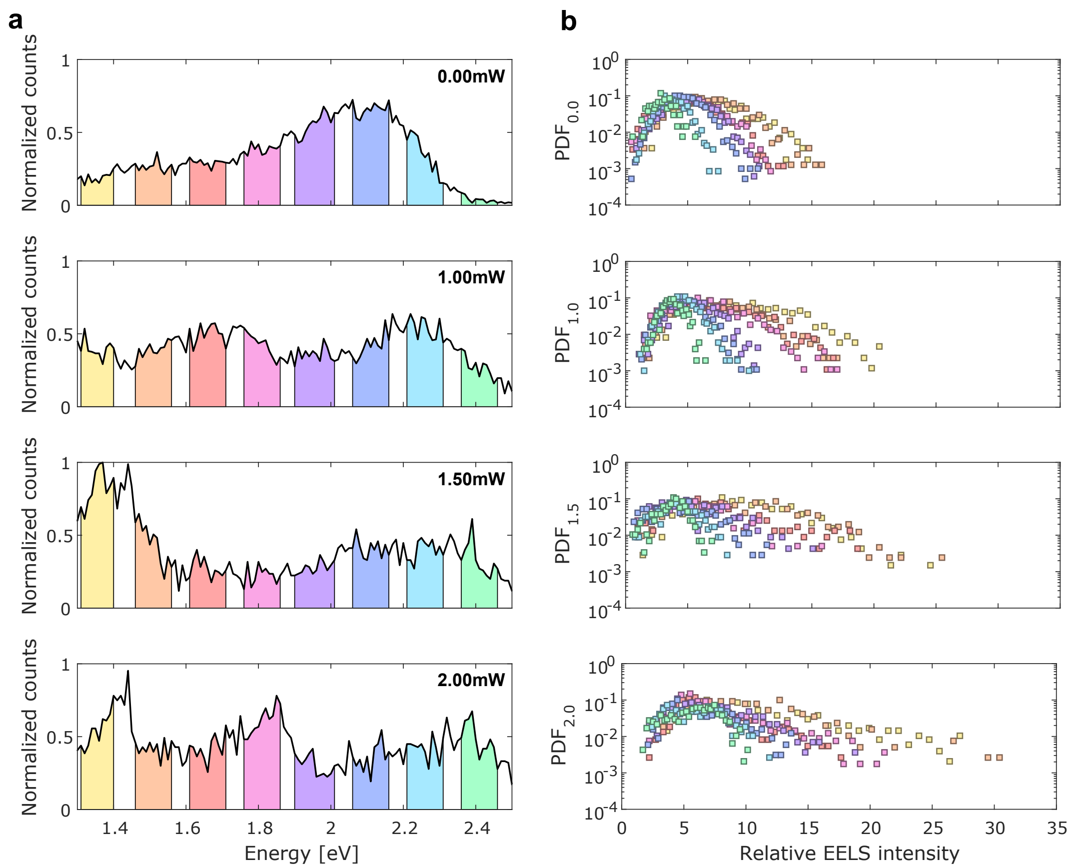

Supplementary Figure 5: Mode distribution 7 nm. **(a)** Normalized histograms of identified central energies of plasmonic peaks from the full spectral image of the 7 nm film with different powers of optical illumination. **(b)** PDFs of relative EELS intensities. The dataset of **(a)** has been discretized into several 0.1 eV windows, and PDFs have been constructed from the intensities of peaks in these ranges.

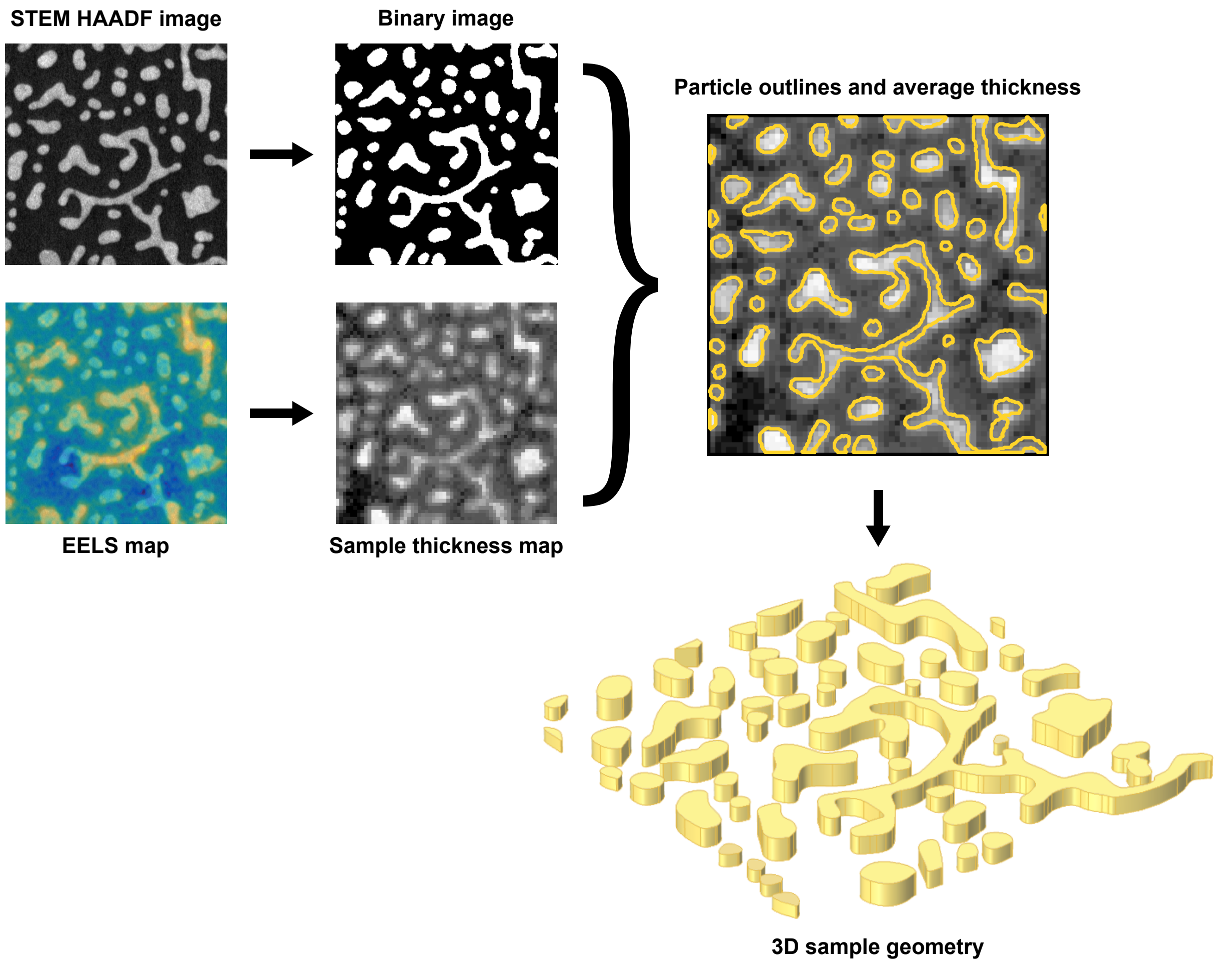

Supplementary Figure 6: Simulation geometries. Overview of the process to generate the thin film geometries used in simulations. The dark-field STEM images are converted to binaries to recover the particle outlines, and the EELS data is integrated in order to construct relative thickness maps of the samples. Using the thickness map and the particle outlines, an average thickness of each gold particle is found and the sample geometry can be constructed.

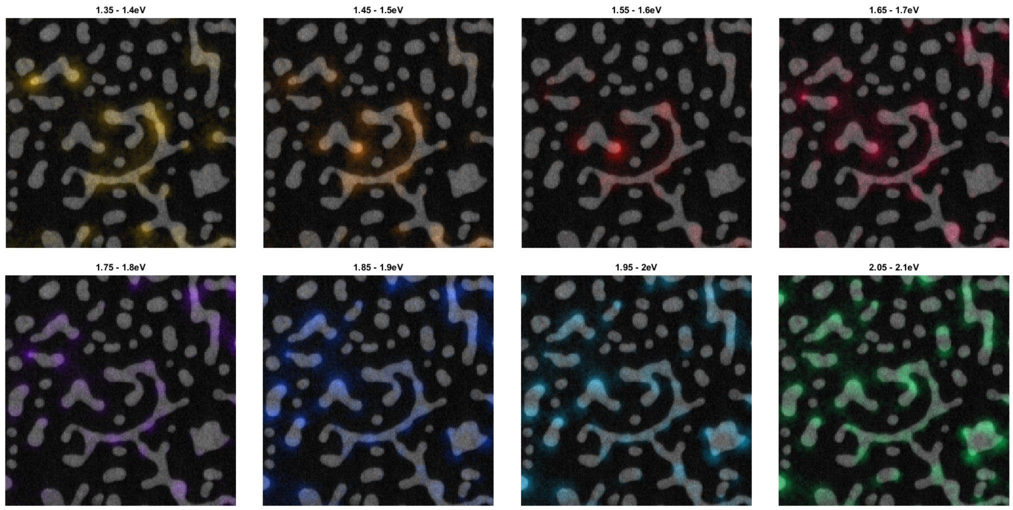

Supplementary Figure 7: EELS maps, y-polarized sample. Integrated EELS data in several energy ranges super imposed on STEM-images for initial 5 nm sample illuminated with 1.5 mW with y-polarization.

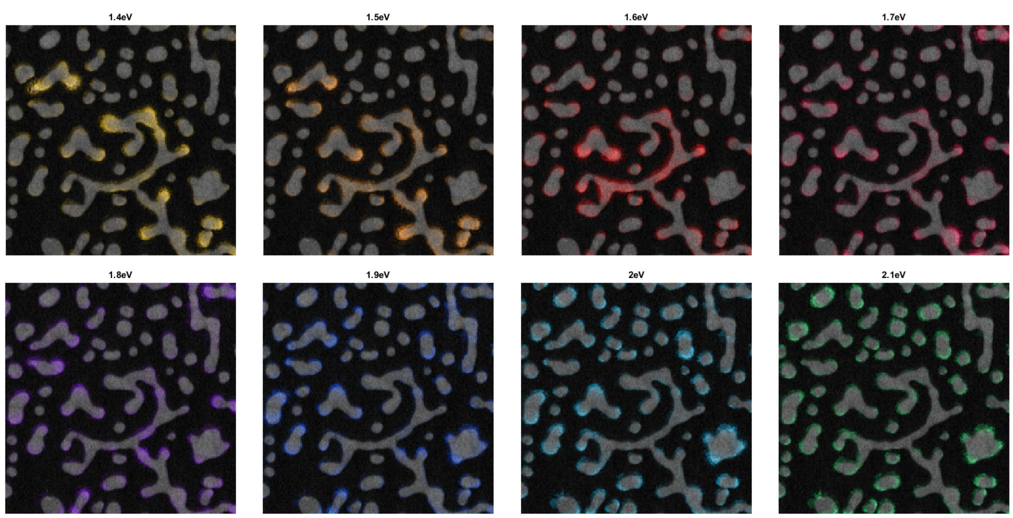

Supplementary Figure 8: Simulated fields. y-polarized sample. Norm of simulated electric field z-components for extracted geometries superimposed on the STEM-images of the sample.

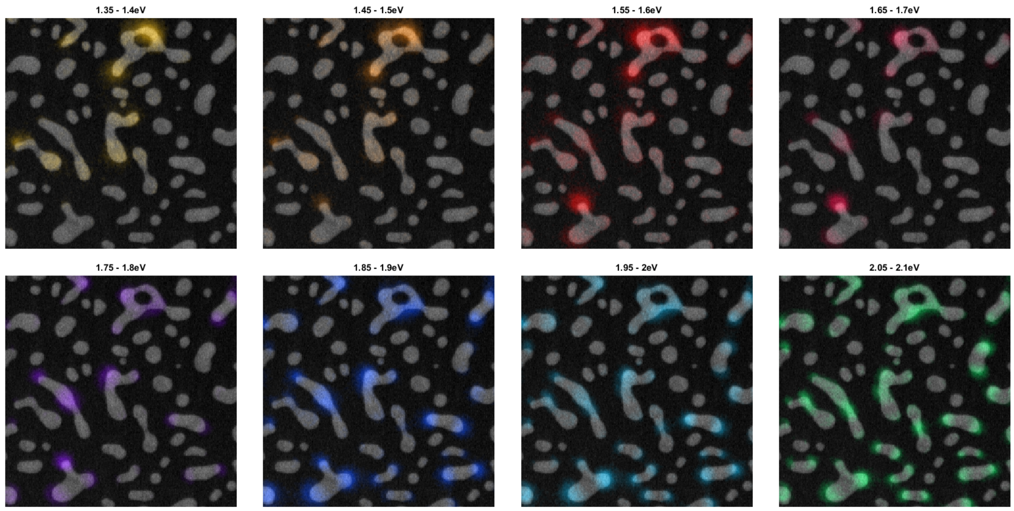

Supplementary Figure 9: EELS maps, x-polarized sample. Integrated EELS data in several energy ranges super imposed on STEM-images for initial 5 nm sample illuminated with 1.5 mW with x-polarization.

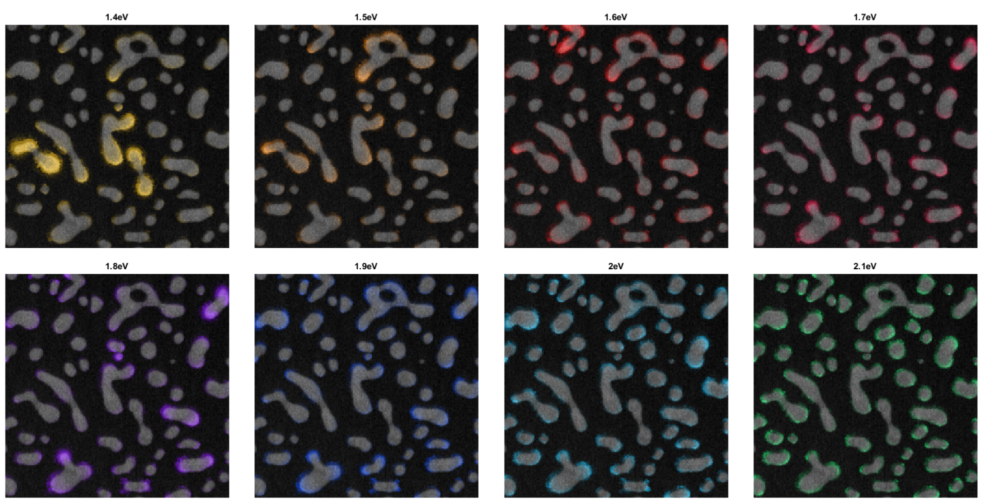

Supplementary Figure 10: Simulated fields. x-polarized sample. Norm of simulated electric field z-components for extracted geometries superimposed on the STEM-images of the sample.

Supplementary discussion

Sample morphologies. The illuminated and intrinsic regions of the films are investigated with a scanning transmission electron microscope (STEM), where we image the films with the high angle annular dark-field (HAADF) detector. From our HAADF images we are able to characterize the morphologies of these films and their filling fractions (see supplementary methods), as well as how these evolve with the different powers used for inducing optical damage to the samples. From (Fig. 1a,b) we get an indication of the fractal nature of the gold particles in the film morphologies across different size scales. If self-similarity is preserved for increasing particle sizes, then the perimeter per area ratio is also preserved and the points will fall along a linear expression. The slope of this expression will give us a quantitative measure of the tortuosity of the system, and we can extract the slope via a linear regression. A system of perfectly separated disks will have a slope of 0.5 perimeter per area, while for increasingly tortuous systems the slope will increase as the particle perimeter grows faster than the particle area. From the 5 and 6 nm films we see that we get two regimes of particle shapes. The smallest particles are falling almost perfectly on the calculated line for circular particles, while above a certain size the particles start to form serpentine structures. We find generally that tortuosity is preserved for the optically reconfigured samples, only decreasing for higher power laser writing. We observe a general trend toward larger circular particles for increasing laser powers. We explain this from the morphologies displayed in Fig. 1.c,d,e, where we see a larger fraction of particles being affected by the laser at higher powers. The surface tension in the molten gold particles, and the high wetting angle of gold on silica, will tend toward spherizing the particles to minimize their surface energies[1,2]. Since the 7 nm sample consists of only one connected cluster the same type of analysis has not been possible.

Supplementary Methods

Sample morphology analysis. 8-bit greyscale HAADF STEM images of a $986 \times 986\,\mathrm{nm}^2$ sample area with 512×512 pixel resolution were used for the image analysis. A histogram of the greyscale distribution was constructed for each image, and the minimum between the majority dark and majority light parts of the image was used as a threshold for converting the images to black and white binaries. A median filter with a 4×4 pixel neighbourhood was applied to the binary images to smoothen the particle outlines, and particles touching the borders of the images were excluded from the analysis. The surface areas and perimeters of the particles were then determined using the particle analysis toolbox in imageJ. The distance of the data points to the theoretical expression for perfectly circular particles was calculated for each data point, and the points closest to the circle line were excluded from the linear fits to find the loglog-slope of the datasets.

Supplementary References

1. Kojima, Y. & Kato, T. Nanoparticle formation in au thin films by electron-beam-induced dewetting. *Nanotechnology* **19**, 255605 (2008).

2. Greene, J. E. Thin film nucleation, growth, and microstructural evolution: An atomic scale view. In Martin, P. M. (ed.) *Handbook of Deposition Technologies for Films and Coatings*, chap. 12, 554–620 (William Andrew Publishing, Boston, 2010), 3 edn.